

---

# Regressor-free Molecule Generation to Support Drug Response Prediction

---

**Kun Li**

School of Computer Science  
Wuhan University  
li\_kun@whu.edu.cn

**Xiuwen Gong**

University of Technology Sydney  
gongxiuwen@gmail.com

**Shirui Pan**

School of Information and Communication Technology  
Griffith University  
s.pan@griffith.edu.au

**Jia Wu**

School of Computing  
Macquarie University  
Jia.wu@mq.edu.au

**Bo Du**

School of Computer Science  
Wuhan University  
gunspace@163.com

**Wenbin Hu \***

School of Computer Science  
Wuhan University  
hwb@whu.edu.cn

## Abstract

Drug response prediction (DRP) is a crucial phase in drug discovery, and the most important metric for its evaluation is the IC<sub>50</sub> score. DRP results are heavily dependent on the quality of the generated molecules. Existing molecule generation methods typically employ classifier-based guidance, enabling sampling within the IC<sub>50</sub> classification range. However, these methods fail to ensure the sampling space range's effectiveness, generating numerous ineffective molecules. Through experimental and theoretical study, we hypothesize that conditional generation based on the target IC<sub>50</sub> score can obtain a more effective sampling space. As a result, we introduce regressor-free guidance molecule generation to ensure sampling within a more effective space and support DRP. Regressor-free guidance combines a diffusion model's score estimation with a regression controller model's gradient based on number labels. To effectively map regression labels between drugs and cell lines, we design a common-sense numerical knowledge graph that constrains the order of text representations. Experimental results on the real-world dataset for the DRP task demonstrate our method's effectiveness in drug discovery. The code is available at: <https://anonymous.4open.science/r/RMCD-DBD1>.

## 1 Introduction

Drug response prediction (DRP) is crucial in drug discovery [14]. It evaluates drug response in cell lines to aid the screening potential pharmacologically active compounds. However, the challenge in drug discovery arises from the large and discrete chemical molecule search space [35]. Specifically, the possible structural scale of drug-like compounds ranges from  $10^{23}$  to  $10^{60}$ , but a small percentage of these (about  $10^8$ ) are therapeutically relevant [37, 11]. Traditional drug discovery techniques typically involve screening large molecule libraries, resulting in a low probability of finding molecules with an adequate efficacy for specific cell lines.

---

\*Corresponding author

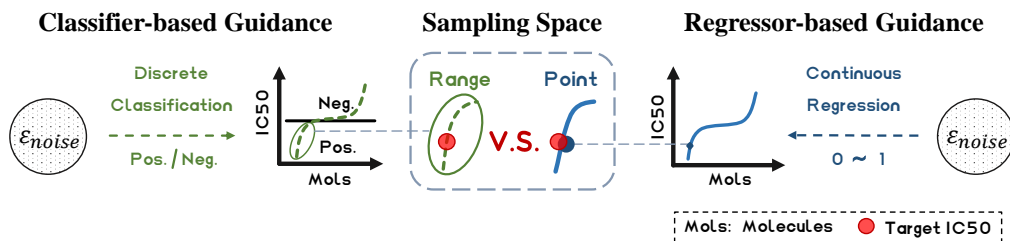


Figure 1: Sampling space comparison for target conditions in classifier- vs. regressor-based guidance molecule generation.

Moreover, molecule quality directly impacts drug screening efficiency and progress during DRP tasks. Typically, high-quality molecules exhibit enhanced pharmacological properties and are more likely to become effective drug candidates. Therefore, generating high-quality molecules has become a core issue in current drug discovery research. With the development of artificial intelligence technology, various molecule generation methods have been proposed, including sequence-based generative models [7], variational auto-encoders [20, 32], normalizing flows [34, 31], and diffusion [15, 22, 13]. Existing molecule generation methods can generate molecules with specific stability and novelty, providing a larger library of virtual screening molecules for drug discovery.

To meet the DRP-based screening tasks’ demands, diffusion-based conditional generation methods have garnered significant attention due to ability to generate specific molecules while maintaining result diversity and novelty. As shown in Fig. 1, traditional diffusion models can generate molecules under certain conditions [15, 25, 50], which are mostly classifier-based [9] (detailed related work is referenced in Appendix B). However, drugs’ features are mostly continuous and quantifiable [33, 8]. The sampling space range guided by the classifier (i.e., whether there is a reaction between the drug and the cell line) is relatively large, hindering its ability to perform precise molecular feature space sampling. In contrast, the diffusion model guided by regressor-based conditions can obtain samples within a narrower range near specific response values. This ensures that the generated molecules are consistent with the target response values, instead of falling within a broader response range. As a result, when generating an identical number of molecules, the number of molecules meeting a given criteria generated using regressor-based guidance is higher than those generated with classifier-based guidance. This improves generation efficiency and increases the drug discovery success rate.

To achieve this, we propose the *regressor-free guided molecule generation* method to ensure sampling within a more effective space, supporting the DRP task. To avoid potential gradient-based adversarial attacks, we opt for a regressor-free guidance method, inspired by classifier-free guidance [12]. Regressor-free guidance is a score-based diffusion scheme, that incorporates a regression controller model, which is based on the number label, into a generative stochastic differential equation (SDE) with a conditional hyperparameter. To effectively map the labels between the drug and the cell line, we create a regression controller model that converts the drug information labels into text with a common-sense numerical knowledge graph (CN-KG). The CN-KG restricts the text representation order. Moreover, since the DRP dataset contains only a limited variety of molecules, training solely on this small dataset can significantly impact the sampling effectiveness. Therefore, we propose a dual-branch controlled noise prediction (DBControl) model to ensure the diffusion processing and sampling effectiveness. The control model is designed for score estimation and consists of two identical graph neural networks (GNNs) connected by zero convolution layers. These convolution layers are gradually added to learn various conditional controls, ensuring the DRP task’s effectiveness.

The experimental results on the GDSCv2 [49] dataset for the DRP task demonstrate our method’s effectiveness in de novo drug design. **This paper’s main contributions are summarized as follows:**

- Regressor-free guidance molecule generation is proposed to ensure sampling within a more effective space. Regressor-free guidance is a score-based diffusion scheme, that incorporates a regression controller model, which is based on the number label, into a generative SDE with a conditional hyperparameter.

- To enhance noise prediction performance, we introduce the DBControl model for score estimation. The control model consists of two GNN-based branches, each undergoing unconditional and conditional mixed training, respectively.
- The experimental results demonstrate that our method outperforms state-of-the-art baselines in conditional molecular graph generation for the DRP task. Furthermore, we validate our method’s effectiveness.

## 2 Methods

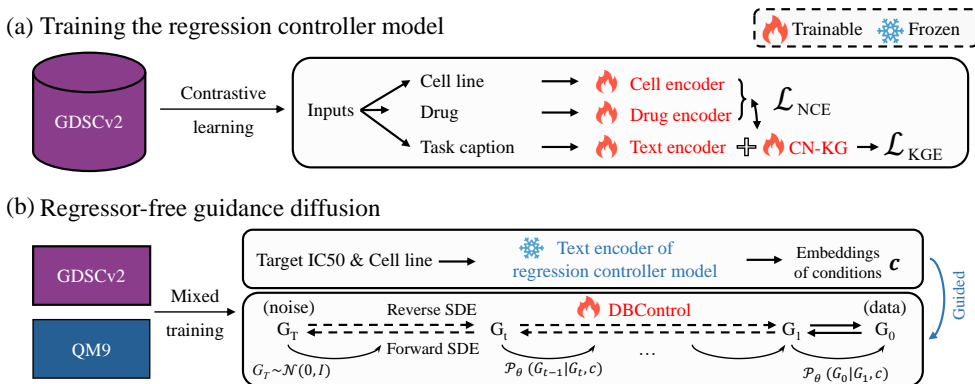


Figure 2: (a) illustrates the training process of the regression controller model, which serves as a conditional encoder guiding diffusion. (b) depicts the regressor-free guidance diffusion process, utilizing the text encoder of the trained regression controller model to encode the target conditions. The DBControl model is a score-based noise prediction model trained on a mixture of the conditional GDSCv2 and unconditional QM9 dataset.

### 2.1 Notations

**Molecular graph representation.** The molecule can be represented as a graph  $\mathbf{G} = (\mathbf{X}, \mathbf{A}) \in \mathbb{R}^{N \times F} \times \mathbb{R}^{N \times N} := \mathcal{G}$ , where  $\mathbf{X}$  and  $\mathbf{A}$  are the node features and weighted adjacency matrix of the graph  $\mathbf{G}$  with  $N$  nodes.  $\mathbf{X}$  is the node feature matrix for atom types described by  $F$ -dimensional one-hot encoding.

**Score-based graph generation.** Based on the seminal work of [42], Graph Diffusion via the System of SDEs (GDSS) was introduced [21]. GDSS utilizes two SDE models to simulate node feature and adjacency matrix diffusion, thereby capturing the complex dependencies between nodes and edges. Thus, the forward diffusion for a graph  $\mathbf{G}$  is defined by an Itô SDE:

$$d\mathbf{G}_t = \mathbf{f}_t(\mathbf{G}_t)dt + \mathbf{g}_t(\mathbf{G}_t)d\mathbf{w}, \quad \mathbf{G}_0 \sim p_{data} \quad (1)$$

where  $\mathbf{f}_t(\cdot) : \mathcal{G} \rightarrow \mathcal{G}$  is the linear drift coefficient,  $\mathbf{g}_t(\cdot) : \mathcal{G} \rightarrow \mathcal{G} \times \mathcal{G}$  is the diffusion coefficient, and  $\mathbf{w}$  is the standard Wiener process. The  $t$ -subscript denotes a time function:  $F_t(\cdot) := F(\cdot, t)$ , which  $t \in [0, T]$ . If the initial state distribution is supposed as  $p_0(\mathbf{G}_0|\mathbf{c})$ , the density at time  $t$  is  $p_t(\mathbf{G}_t|\mathbf{c})$  when conditioned on  $\mathbf{c}$ . Therefore, the reverse-time SDE from  $T$  to 0 corresponding to Eq. 1 is given by [1]:

$$d\mathbf{G}_t = \{\mathbf{f}_t(\mathbf{G}_t) - g_t^2 [\nabla_{\mathcal{G}} \log p_t(\mathbf{G}) + \nabla_{\mathcal{G}} \log p_t(\mathbf{c}|\mathbf{G}_t)]\} d\bar{t} + g_t d\bar{\mathbf{w}}, \quad (2)$$

where  $\nabla_{\mathcal{G}} \log p_t(\mathbf{G}_t)$  is the graph score function and  $\bar{\mathbf{w}}_t$  represents the reverse-time standard Wiener process. The marginal distribution under forward diffusion is denoted as  $p_t$ , and the corresponding reverse diffusion process can be described by the following SDEs, which describe the diffusion process of each component,  $\mathbf{X}$  and  $\mathbf{A}$ , respectively:

$$\begin{cases} d\mathbf{X}_t = [\mathbf{f}_{1,t}(\mathbf{X}_t) - g_{1,t}^2 \nabla_{\mathbf{X}_t} \log p_t(\mathbf{X}_t, \mathbf{A}_t)] d\bar{t} + g_{1,t} d\bar{\mathbf{w}}_1 \\ d\mathbf{A}_t = [\mathbf{f}_{2,t}(\mathbf{A}_t) - g_{2,t}^2 \nabla_{\mathbf{A}_t} \log p_t(\mathbf{X}_t, \mathbf{A}_t)] d\bar{t} + g_{2,t} d\bar{\mathbf{w}}_2 \end{cases} \quad (3)$$

where  $\mathbf{f}_{1,t}$  and  $\mathbf{f}_{2,t}$  are linear drift coefficients satisfying  $\mathbf{f}_t(\mathbf{X}, \mathbf{A}) = (\mathbf{f}_{1,t}(\mathbf{X}), \mathbf{f}_{2,t}(\mathbf{A}))$ ,  $g_{1,t}$  and  $g_{2,t}$  are scalar diffusion coefficients, and  $\bar{\mathbf{w}}_1, \bar{\mathbf{w}}_2$  are reverse-time standard Wiener processes.

## 2.2 Method overview

In this paper, we introduced a regressor-free guidance molecule generation method to ensure sampling within a more effective space, which can support the DRP task. Our method mainly consists of two models: the regression controller model for guiding conditional generation and the DBControl model for score estimation. Our method’s framework is shown in Fig. 2. In the diffusion phase, the DBControl model was used for noise prediction. First, DBControl is trained using molecular datasets such as QM9 [39] and ZINC250k [17]. Then, the regression controller model was trained on the GDSCv2 dataset for the DRP task (i.e., approximately 1% of the molecule number in the unconditional molecule dataset). Finally, the DBControl model was trained on a mixture of the GDSCv2 and unconditional molecular datasets.

### 2.2.1 The regression controller model

With the regression controller model, a natural language process description on the molecule with the cell line is taken as the text input, and molecule and cell line regular representation (e.g., sequence and motifs encoding) is used as the regular input. Then, the natural language description is generated using templates as follows:

$$\text{The response value of the drug with the [name of the cell line] is [IC}_{50}], \quad (4)$$

where [name of the cell line] refers to the name of the specific cell line, and [IC<sub>50</sub>] represents the specific IC<sub>50</sub> score. IC<sub>50</sub> stands for Half Maximal Inhibitory Concentration, which is commonly used to measure the biological activity of a drug. In this instance, the IC<sub>50</sub> score is a concrete number, such as, "zero five two one" means that the IC<sub>50</sub> score is 0.521. Furthermore, we used text to describe the value, instead of a string of numbers, such as "0.521". The generated numeric text retains a fixed precision (e.g., 0.521 has a precision of  $\xi = 3$ ); the number of valid digits is  $\xi \in \mathbb{N}$ .

Various drug and cell line representation methods exist, such as GNNs [22] and the transformer [18]. The regression controller model proposed in this paper has no restriction in this regard; hence, it is not specified. In addition, the regular representation branch is denoted by  $\Phi_f$  and the transformer-based textual description branch is  $\Phi_{\text{cap}}$ . The  $\Phi_{\text{cap}}$  input is the target IC<sub>50</sub> scores and cell lines, denoted as  $c = (\mathbf{X}_{\text{cell}}, \mathbf{X}_{\text{number}})$ . We normalized the feature vectors in a hyper-sphere using  $u_i := \frac{\Phi_f(\text{Drug}, \mathbf{X})}{\|\Phi_f(\text{Drug}, \mathbf{X})\|}$  and  $v_j := \frac{\Phi_{\text{cap}}(\mathbf{X}_{\text{cell}}, \mathbf{X}_{\text{number}})}{\|\Phi_{\text{cap}}(\mathbf{X}_{\text{cell}}, \mathbf{X}_{\text{number}})\|}$ . Then, the similarity between  $u_i$  and  $v_j$  was calculated as  $u_i^T v_j$ . Finally, the contrast learning between the two branches was optimized by the supervised contrastive loss function.

$$\mathcal{L}_{\text{NCE}} = -\frac{1}{N} \left( \sum_i \log \frac{\exp(u_i^T v_i / \sigma)}{\sum_{j=1}^N \exp(u_i^T v_j / \sigma)} + \sum_i \log \frac{\exp(v_i^T u_i / \sigma)}{\sum_{j=1}^N \exp(v_i^T u_j / \sigma)} \right), \quad (5)$$

where,  $N$  is the batch size, and  $\sigma$  is the temperature value used for scaling the logits.

Therefore, to enable the text module to represent the numerical labels at the standard ordered cognition level, we introduced the CN-KG [27] to enhance the ordered representation of numerical texts. The CN-KG has natural number entities, denoted as  $E \subseteq \mathbb{N}^*$ . The  $E$  entities are linked by a single relationship type called "is less than," denoted as  $L$ , which ensures that number transfer properties are captured. Furthermore, the margin-based loss function  $\mathcal{L}_{\text{KGE}}$  was used for the CN-KG embedding. We aimed to minimize the differences in embedding vectors between the entities’ set  $E$  and the single relationship  $L$  (i.e. is less than)

$$\mathcal{L}_{\text{KGE}} = \sum_{(h,l,t) \in S} [\gamma + d(\mathbf{h} + \mathbf{l}, \mathbf{t}) - d(\mathbf{t} + \mathbf{l}, \mathbf{h})]_+, \quad (6)$$

where,  $[x]_+$  denotes the positive part of  $x$ ,  $\gamma > 0$ , and is a margin hyperparameter. The set  $S$  is composed of the triplets  $(h, l, t)$ , with  $h, t \in E, l \in L$ . Also, the embeddings  $\mathbf{h}, \mathbf{l}, \mathbf{t}$  obtained values

in  $\mathbb{R}^k$  (i.e.,  $k$  is a hyperparameter) using the transformer-based number encoder and are denoted with the same letters in bold characters. In addition, the  $L_1$ - or  $L_2$ -norm can be used for the similarity measure  $d(\cdot)$ . To ensure the effectiveness of  $\mathcal{L}_{\text{KGE}}$ ,  $\mathbf{1}$  is represented by a matrix filled with ones, and its parameters are not trained. Finally, the regression controller model’s goal is to jointly optimize the following contrast and CN-KG embedding loss functions:

$$\mathcal{L} = \alpha \mathcal{L}_{\text{NCE}} + (1 - \alpha) \mathcal{L}_{\text{KGE}}, \quad (7)$$

where  $\alpha$  represents the joint optimization weight adjustment factor for the two loss functions.

## 2.2.2 The dual-branch controlled noise prediction model

The limited diversity of molecular distributions in a specific task may lead to the poor performance of noise prediction networks trained on small molecular datasets. To ensure that the network adapts to the molecular and conditional distributions in a new task while remembering the prior knowledge, we proposed the dual-branch controlled noise prediction model, named DBControl. The DBControl model consists of two structurally consistent GNNs (i.e., the two networks denoted as  $B_1$  and  $B_2$ , detailed structural diagrams can be found in the Appendix 5).  $B_1$  participates in unconditional molecule training while  $B_2$  does not. During the conditional mixed training phase,  $B_2$  obtains its weights from  $B_1$  for encoding conditional features. Notably,  $B_1$  and  $B_2$  weights must be optimized simultaneously, instead of simply freezing  $B_1$  [51].

We represented conditional information  $\mathbf{c}$  via  $\Phi_{\text{cap}}$  to obtain  $\mathbf{C}$  (see Section 2.2.1). For time  $t$ , two DBControl models  $B_\phi = (B_{\phi,1}, B_{\phi,2})$  and  $B_\theta = (B_{\theta,1}, B_{\theta,2})$  were proposed to estimate scores  $\nabla_{\mathbf{A}} \log p_t(\mathbf{X}_t, \mathbf{A}_t, \mathbf{C}_t)$  and  $\nabla_{\mathbf{X}} \log p_t(\mathbf{X}_t, \mathbf{A}_t, \mathbf{C}_t)$ , respectively, expressed as follows:

$$\begin{cases} \mathbf{X}^{l+1}, \mathbf{A}^{l+1} = B_{\phi,1}^l(\mathbf{X}^l, \mathbf{A}^l) + \mathcal{Z}(B_{\phi,2}^l(\mathbf{X}^l + \mathcal{Z}(\mathbf{C}^l) - \overline{\mathcal{Z}}(\mathbf{C}^{l-1}), \mathbf{A}^l + \mathcal{Z}(\mathbf{C}^l) - \overline{\mathcal{Z}}(\mathbf{C}^{l-1}))) \\ \mathbf{X}^{l+1} = B_{\theta,1}^l(\mathbf{X}^l, \mathbf{A}^l) + \mathcal{Z}(B_{\theta,2}^l(\mathbf{X}^l + \mathcal{Z}(\mathbf{C}^l) - \overline{\mathcal{Z}}(\mathbf{C}^{l-1} + \delta(t)), \mathbf{A}^l)) \end{cases} \quad (8)$$

where  $\mathcal{Z}(\cdot)$  and  $\overline{\mathcal{Z}}(\cdot)$  are zero convolutional layers, and  $\mathbf{C}^l = \mathbf{0}$  when  $l = 1$  (where  $l$  represents the number of GNN layers).

**Regressor-free guidance diffusion.** Classifier guidance diffusion methods are typically insufficient for the DRP task (the algorithm is referenced in Algorithm 1). Hence, we proposed the regressor-free guidance molecule generation method to support DRP. To guide the generation process towards the desired conditioning information  $\mathbf{c}$  for sampling, one can sample from a conditional distribution  $q_0(\mathbf{G}|\mathbf{c})$ . The expectations are carried over to the samples  $\mathbf{G}_0 \sim p_{\text{data}}$  and  $\mathbf{G}_t \sim p_{0t}(\mathbf{G}_t|\mathbf{G}_0, \mathbf{c})$ . Therefore, the transition probability  $p_{0t}(\mathbf{G}_t|\mathbf{G}_0, \mathbf{c})$  can be represented as follows:

$$p_{0t}(\mathbf{G}_t|\mathbf{G}_0, \mathbf{c}) = p_{0t}(\mathbf{X}_t|\mathbf{X}_0, \mathbf{c})p_{0t}(\mathbf{A}_t|\mathbf{A}_0, \mathbf{c}). \quad (9)$$

Then, to minimize the Euclidean distance, we introduced the objectives that generalize the score matching [42] to estimate the scores as follows:

$$\begin{aligned} & \min_{\theta} \mathbb{E}_t \left\{ \lambda_1(t) \mathbb{E}_{\mathbf{G}_0} \mathbb{E}_{\mathbf{G}_t|\mathbf{G}_0} \|B_{\theta,t}(\mathbf{G}_t, \mathbf{c}) - \nabla_{\mathbf{X}_t} \log p_{0t}(\mathbf{X}_t|\mathbf{X}_0, \mathbf{c})\|_2^2 \right\}, \\ & \min_{\phi} \mathbb{E}_t \left\{ \lambda_2(t) \mathbb{E}_{\mathbf{G}_0} \mathbb{E}_{\mathbf{G}_t|\mathbf{G}_0} \|B_{\phi,t}(\mathbf{G}_t, \mathbf{c}) - \nabla_{\mathbf{A}_t} \log p_{0t}(\mathbf{A}_t|\mathbf{A}_0, \mathbf{c})\|_2^2 \right\}, \end{aligned} \quad (10)$$

where  $\lambda_1(t)$  and  $\lambda_2(t)$  are positive weighting functions. The expectations in Eq. 10 can be efficiently computed using the Monte Carlo estimate with the samples  $(t, \mathbf{c}, \mathbf{G}_0, \mathbf{G}_t)$  [21].

**Regressor-free guidance sampling.** Let  $\mathbf{G} \leftarrow (\mathbf{X} \sim \mathcal{N}(\mathbf{0}, \mathbf{I}), \mathbf{A} \sim \mathcal{N}(\mathbf{0}, \mathbf{I}))$ ,  $\mathbf{z} = \{\mathbf{z}_\lambda \mid \lambda \in [\lambda_{\text{min}}, \lambda_{\text{max}}]\}$  for hyperparameters  $\lambda_{\text{min}} < \lambda_{\text{max}} \in \mathbb{R}$ , which  $\mathbf{z}_\lambda = \alpha_\lambda \mathbf{G} + \sigma_\lambda \epsilon$ . Then, trained DBControl models  $B_\phi$  and  $B_\theta$  can simulate the system of reverse-time SDEs Eq.3 to enable the reverse-time diffusion process as a generative model. The two DBControl models used for estimating true scores  $\nabla_{\mathbf{X}} \log p_t(\mathbf{X}|\mathbf{c})$  and  $\nabla_{\mathbf{A}} \log p_t(\mathbf{A}|\mathbf{c})$  respectively are abbreviated as  $\epsilon_\theta(\mathbf{z}_\lambda, \mathbf{c})$ . In the conditional mixed training phase, when unconditional data are the input,  $\mathbf{c}$  are labeled as empty

text  $\emptyset$ , denoted as  $\epsilon_{\theta}(\mathbf{z}_{\lambda}, \emptyset)$ . Based on the Eq. 2, the score estimation is calculated using a conditional and unconditional linear combination when sampling:

$$\tilde{\epsilon}_{\theta}(\mathbf{z}_{\lambda}, \mathbf{c}) = (1 + w)\epsilon_{\theta}(\mathbf{z}_{\lambda}, \mathbf{c}) - w\epsilon_{\theta}(\mathbf{z}_{\lambda}, \emptyset), \quad (11)$$

where  $w$  is a conditional control strength parameter ( $w > 0$ ), and  $w = 0$  indicates unconditional generation.  $\tilde{\epsilon}_{\theta}(\mathbf{z}_{\lambda}, \mathbf{c})$  is then used in place of  $\epsilon_{\theta}(\mathbf{z}_{\lambda}, \mathbf{c})$  when sampling, resulting in approximate samples from the distribution  $\tilde{p}_t(\mathbf{z}_{\lambda}, \mathbf{c}) \propto p_t(\mathbf{z}_{\lambda}, \mathbf{c})p_t(\mathbf{c}, \mathbf{z}_{\lambda})^w$ . The sampling algorithm is referenced in Algorithm 2.

---

**Algorithm 1** Joint training the DBControl model with regressor-free guidance

---

**Require:** molecular data for the specific task  $\{\mathbf{G}_0 = (\mathbf{X}_0, \mathbf{A}_0), \mathbf{c}\}$ , the DBControl models  $\epsilon_{\theta}$ , condition embedding model  $f_{\theta}$ , schedule function  $\delta(\cdot)$ ,  $\alpha(\cdot)$  and  $\sigma(\cdot)$

- 1: **repeat**
  - 2:   Sample  $t \sim \mathcal{U}(0, 1]$ ,  $\epsilon_{\mathbf{X}} \sim \mathcal{N}(\mathbf{0}, \mathbf{I})$ ,  $\epsilon_{\mathbf{A}} \sim \mathcal{N}(\mathbf{0}, \mathbf{I})$
  - 3:    $\mathbf{T}_0 \leftarrow \emptyset$ ,  $\mathbf{N}_0 \leftarrow \emptyset$  with definite probability
  - 4:    $\mathbf{C}_t = \delta(t)\mathbf{f}_{\theta}(\mathbf{c})$  ▷ Embedding the regression values as conditions
  - 5:    $\mathbf{G}_t = (\mathbf{X}_t, \mathbf{A}_t) \leftarrow (\alpha(t)\mathbf{X}_0 + \sigma(t)\epsilon_{\mathbf{X}}, \alpha(t)\mathbf{A}_0 + \sigma(t)\epsilon_{\mathbf{A}})$
  - 6:    $\epsilon_{\theta}^{\mathbf{X}}, \epsilon_{\theta}^{\mathbf{A}} \leftarrow \epsilon_{\theta}(\mathbf{G}_t, \mathbf{A}_t, \mathbf{C}_t, t)$  ▷ Regressor-free guidance generation
  - 7:   Minimize  $\|\epsilon_{\theta}^{\mathbf{X}} - \epsilon_{\mathbf{X}}\|_2^2 + \|\epsilon_{\theta}^{\mathbf{A}} - \epsilon_{\mathbf{A}}\|_2^2$
  - 8: **until** converged
- 

---

**Algorithm 2** Conditional sampling with regressor-free guidance

---

**Require:** number of time steps  $N$ , the DBControl models  $\epsilon_{\theta}$ , drift coefficient function  $f(\cdot)$ , diffusion coefficient function  $g(\cdot)$ , schedule function  $\sigma(\cdot)$ , post-processing function  $post(\cdot)$ , conditioning information for conditional sampling  $\mathbf{c}$ , condition embedding model  $f_{\theta}$

- 1: Sample initial graph  $\mathbf{G} \leftarrow (\mathbf{X} \sim \mathcal{N}(\mathbf{0}, \mathbf{I}), \mathbf{A} \sim \mathcal{N}(\mathbf{0}, \mathbf{I}))$
  - 2:  $\Delta t = \frac{T}{N}$
  - 3: **for**  $i \leftarrow N$  to 1 **do**
  - 4:    $\epsilon_{\mathbf{X}} \sim \mathcal{N}(\mathbf{0}, \mathbf{I})$ ,  $\epsilon_{\mathbf{A}} \sim \mathcal{N}(\mathbf{0}, \mathbf{I})$
  - 5:    $t \leftarrow i\Delta t$
  - 6:    $\mathbf{C} = \delta(t)\mathbf{f}_{\theta}(\mathbf{c})$  ▷ Embedding the regression values as conditions
  - 7:    $\epsilon_{\theta}^{\mathbf{X}}, \epsilon_{\theta}^{\mathbf{A}} \leftarrow (1 + w)\epsilon_{\theta}(\mathbf{G}, \mathbf{A}, \mathbf{C}, t) - w\epsilon_{\theta}(\mathbf{G}, \mathbf{A}, \emptyset, t)$  ▷ Regressor-free guidance sampling
  - 8:    $\mathbf{X} \leftarrow \mathbf{X} - (f(t)\mathbf{X} + \frac{g(t)^2}{\sigma(t)}\epsilon_{\theta}^{\mathbf{X}})\Delta t + g(t)\sqrt{\Delta t}\epsilon_{\mathbf{X}}$
  - 9:    $\mathbf{A} \leftarrow \mathbf{A} - (f(t)\mathbf{A} + \frac{g(t)^2}{\sigma(t)}\epsilon_{\theta}^{\mathbf{A}})\Delta t + g(t)\sqrt{\Delta t}\epsilon_{\mathbf{A}}$
  - 10: **end for**
  - 11: **return**  $post(\mathbf{X}, \mathbf{A})$
- 

### 3 Theoretical discussion

In this section, we first address why the regressor-free guidance sampling method is more effective than the classifier-based guidance sampling for molecules. Second, we aim to demonstrate the regression controller model’s effectiveness and how it accurately guides the diffusion model to perceive different IC<sub>50</sub> scores when it is used as a condition. The IC<sub>50</sub> scores are represented as continuous values within the range of 0 to 1 after normalization.

**Notations.** Let the classifier’s class threshold be denoted as  $T \in (0, 1)$ , where the conditional input is  $\{0, 1\}$ . The conditional input for the regressor is  $(0, 1)$ , and the target IC<sub>50</sub> score is denoted as  $\mathbf{C}_{\text{aim}} \in \mathbb{R}$ . The classifier and regressor’s errors during supervised training are denoted as  $\varepsilon_1$  and  $\varepsilon_2$ , respectively. Their sampling spaces are  $\mathbf{S}_{cls} = [0 \pm \varepsilon_1, T \pm \varepsilon_1]$  and  $\mathbf{s}_{reg} = \left[ \mathbf{C}_{\text{aim}} - \frac{10^{-\xi}}{2} \pm \varepsilon_2, \mathbf{C}_{\text{aim}} + \frac{10^{-\xi}}{2} \pm \varepsilon_2 \right]$ , where  $0 < \mathbf{C}_{\text{aim}} < T < 1$ . 0 and  $T$  are the upper and lower bounds of the category corresponding to the contained  $\mathbf{C}_{\text{aim}}$ . In addition, the sampling space size is denoted as  $\|\mathbf{S}\|$ . Then, the two sampling space sizes can be represented as  $\|\mathbf{S}_{cls}\|, \|\mathbf{S}_{reg}\|$ .

**Proposition 1 (Main proposition)** For any  $C_{\text{aim}} \in (0, 1)$ , then  $\|S_{cls}\| \geq \|S_{reg}\|$  exists.

Proposition 1 states that the regression point sampling space is smaller than that of the class range (refer to Appendix Proof.1 for detailed proof). The two ranges are equal if  $T = 10^{-\xi}$ . Practically,  $\xi$  is related to the model’s performance. If  $T \leq 10^{-\xi}$ , the  $(0, T)$  collapses to a single point, becoming a regressor-free guidance exception.

Second, we used a regression controller model to convert  $IC_{50}$  into text labels. However, we must demonstrate whether this method can effectively represent  $C_{\text{aim}}$ .  $C_{\text{aim}}$  being effectively represented mathematically means that its representation is unique. Let the number encoder of the regression controller model (see Section 2.2.1) be denoted as  $\Theta(\cdot)$ .

**Proposition 2 (Uniqueness of  $C_{\text{aim}}$  Representation)** For any  $\lambda \in [0, 1]$ , and  $\lambda \neq C_{\text{aim}}$ , then we say that  $\Theta(C_{\text{aim}}) \neq \Theta(\lambda)$ .

Proposition 2 indicates the uniqueness of  $C_{\text{aim}}$  representation via the number encoder  $\Theta(\cdot)$  (refer to Appendix Proof.2 for detailed proof).  $E$  is the entity set of CN-KG and  $L$  is the relationship called "is less than". We mapped  $IC_{50}$  to  $E$  following the definition of a well ordered set [44]. Specifically, given that the  $IC_{50}$  scores in the dataset have a finite decimal precision of  $\xi \in \mathbb{N}$ , we constructed a well-ordered set  $W$  of size  $n$ , where  $n = 10^\xi$ ,  $n \in \mathbb{N}^*$ :

$$W[0] = 0, W[1] = 1, \dots, W[i] = i, W[n] = n, \quad (12)$$

where  $i \in [0, n]$ . Therefore, each element  $W[i]$  is unique, implying that in  $W$ , every  $IC_{50}$  is also unique and corresponds to its representation with precision  $\xi$ . Since  $\Theta(W[i])$ ’s representation is constrained by  $\mathcal{L}_{\text{KGE}}$ , we can construct a well-ordered set  $V$ :

**Proposition 3 (Equal interval representation of  $\Theta$ )** For any  $\xi$ , a perturbation  $\epsilon_3$  exist to make  $\Theta(V[i]) - \Theta(V[i + 1]) = 1 + \epsilon_3$ .

where  $V[i] = \Theta(W[i])$  and  $\epsilon_3 \in \mathbb{R}$  is a model perturbation. **1** is the only relationship in CN-KG, represented as a matrix filled entirely with ones (i.e.,  $\|\mathbf{1}\| = 1$ ), which is not involved in the training. Proposition 3 states that  $V$  is a well-ordered set under ideal conditions (i.e.,  $\epsilon_3$  near to 0, refer to Appendix Proof.3 for detailed proof). As a result, Proposition 2 can be proved due to the uniqueness of the elements in the well-ordered set (See Appendix 2 for details). Therefore, the regression controller model can effectively represent any  $IC_{50}$ .

## 4 Experiments

### 4.1 Experimental setup

We selected the DRP task’s GDSCv2 as the conditional molecular dataset and QM9 as the unconditional dataset (refer to Table 4 and Table 5) for resource consideration. The evaluation metrics include Fréchet chemNet distance (FCD) [38] and Neighborhood subgraph pairwise distance kernel maximum mean discrepancy (NSPDK MMD) [5]. Further details regarding the experimental environment and hyperparameter tuning are detailed in the Appendix D. Error experiments for the method are referenced as Appendix D.5, while visualization-related information is referenced as Appendix E.

### 4.2 Overall experiment

We evaluated whether the molecules generated by our model can accurately predict regression labels and generate molecules under specific conditions. Then, we compared our method with representative molecule generation methods (refer to Appendix D.1 for further details). Tables 1 and 2 display the performance comparison between our model and the mainstream molecule generation models, with the metrics being FCD and MMD.

The TopK refers to the top  $K$  molecules that meet the criteria of a specific cell line and  $IC_{50}$  score. When  $K$  is set to 1, the target molecule is the one that reacts closest to the target  $IC_{50}$  for a specific cell line. Therefore, a smaller  $K$  indicates greater task difficulty. We trained and sampled the recent methods. The results indicate that our model achieved the best performance in all metrics and cell

Table 1: **Results of FCD**. The metric is calculated with 1000 samples generated from each model with the TopK (K=3 / 5 / 10 / 15 / 20). A lower number indicates a better generation quality, and the best performance is highlighted in bold.

Method	ES3, IC <sub>50</sub> =0.4	ES5, IC <sub>50</sub> =0.4	NCI-H187, IC <sub>50</sub> =0.35	Hs-578-T, IC <sub>50</sub> =0.4
GDSS [21]	83.2 / 77.4 / 60.2 / 56.2 / 52.1	72.6 / 65.6 / 58.9 / 55.2 / 58.9	95.1 / 92.5 / 83.8 / 80.2 / 74.0	104.5 / 74.8 / 73.4 / 70.0 / 65.3
EDM [13]	82.9 / 76.3 / 59.8 / 56.7 / 52.9	72.4 / 65.5 / 59.3 / 56.3 / 59.9	94.4 / 91.7 / 83.6 / 80.4 / 74.6	104.5 / 75.5 / 73.8 / 71.0 / 66.3
CDGS [15]	85.0 / 77.8 / 61.1 / 57.4 / 53.1	74.1 / 66.7 / 59.6 / 56.3 / 60.2	95.4 / 93.1 / 84.9 / 81.1 / 74.8	106.6 / 76.7 / 74.4 / 71.0 / 66.5
GeoLDM [47]	84.2 / 78.2 / 61.3 / 57.7 / 53.7	73.9 / 66.9 / 60.2 / 56.7 / 60.2	95.4 / 92.9 / 84.7 / 81.5 / 75.5	105.5 / 76.4 / 74.7 / 71.6 / 67.1
DiGress [45]	85.2 / 77.7 / 60.9 / 57.4 / 53.0	74.3 / 67.4 / 60.1 / 56.9 / 60.4	96.9 / 94.0 / 85.2 / 81.1 / 74.6	106.7 / 77.2 / 74.5 / 71.3 / 66.3
MOOD [25]	80.2 / <b>71.0</b> / 57.7 / 53.8 / 48.7	70.0 / 64.7 / 55.5 / 52.9 / 57.2	92.3 / 88.0 / 77.4 / 75.1 / 69.9	100.8 / 71.4 / <b>67.5</b> / 65.5 / 61.6
GruM-2D [22]	85.3 / 77.4 / 60.7 / 57.1 / 52.7	73.5 / 66.5 / 59.6 / 56.3 / 59.7	97.2 / 94.2 / 84.9 / 80.4 / 74.4	105.5 / 76.3 / 73.9 / 71.0 / 66.3
Ours(w=0)	78.6 / 73.0 / 62.4 / 60.5 / 56.4	69.2 / <b>61.5</b> / 57.5 / 56.3 / 59.8	92.5 / 88.1 / 81.9 / 79.3 / 74.4	99.9 / 72.3 / 72.6 / 70.2 / 66.7
Ours(w=1)	<b>77.0</b> / 72.3 / <b>56.0</b> / <b>52.1</b> / <b>47.8</b>	<b>68.8</b> / 63.3 / <b>53.6</b> / <b>50.7</b> / <b>54.9</b>	<b>90.2</b> / <b>86.2</b> / <b>76.1</b> / <b>74.1</b> / <b>68.5</b>	<b>98.3</b> / <b>68.8</b> / 67.7 / <b>64.3</b> / <b>60.1</b>

Table 2: **Results of MMD**. The remaining setting is the same as in Table 1.

Method	ES3, IC <sub>50</sub> =0.4	ES5, IC <sub>50</sub> =0.4	NCI-H187, IC <sub>50</sub> =0.35	Hs-578-T, IC <sub>50</sub> =0.4
GDSS [21]	.351 / .267 / .150 / .129 / .119	.401 / .277 / .177 / .146 / .133	.433 / .283 / .187 / .163 / .145	.338 / .232 / .177 / .145 / .134
EDM [13]	.338 / .251 / <b>.139</b> / .116 / .106	.382 / .262 / .165 / .134 / .120	.411 / .265 / .172 / .148 / .130	.324 / .222 / .163 / .132 / .121
CDGS [15]	.340 / .255 / .142 / .118 / .110	.391 / .269 / .169 / .137 / .122	<b>.410</b> / .264 / <b>.170</b> / .149 / .131	.326 / .225 / .165 / .134 / .123
GeoLDM [47]	.340 / .255 / .146 / .121 / .113	.385 / .265 / .167 / .137 / .123	.418 / .269 / .176 / .152 / .134	.322 / .223 / .168 / .138 / .125
DiGress [45]	.341 / .255 / .147 / .122 / .113	.386 / .265 / .166 / .137 / .123	.422 / .272 / .178 / .154 / .134	.324 / .223 / .168 / .137 / .124
MOOD [25]	.347 / .242 / .195 / .152 / .144	<b>.304</b> / .229 / .150 / .139 / .131	.463 / .311 / .216 / .174 / .151	.305 / .226 / .180 / .160 / .138
GruM-2D [22]	.337 / .250 / .138 / .116 / .106	.386 / .263 / .164 / .133 / .120	.410 / <b>.263</b> / .172 / .148 / .130	.325 / .220 / .163 / .131 / .121
Ours(w=0)	.387 / .300 / .207 / .184 / .164	.384 / .258 / .177 / .159 / .142	.458 / .297 / .212 / .180 / .159	.334 / .244 / .195 / .164 / .146
Ours(w=1)	<b>.313</b> / <b>.221</b> / .142 / <b>.113</b> / <b>.101</b>	.327 / <b>.226</b> / <b>.135</b> / <b>.116</b> / <b>.107</b>	.428 / .273 / .178 / <b>.146</b> / <b>.123</b>	<b>.299</b> / <b>.200</b> / <b>.158</b> / <b>.129</b> / <b>.109</b>

line tasks. Specifically, the FCD and MMD were 2.68% and 2.23% higher than the best model, respectively. Furthermore, numerical values cannot intuitively demonstrate our method’s superiority. Therefore, we selected four mainstream methods and visualized a set of generation data for the target pair (NCI-H187, IC<sub>50</sub>=0.35). As shown in Fig. 3, the molecules generated by our method are mainly centered around condition sampling, while those from other methods deviate significantly from the target value.

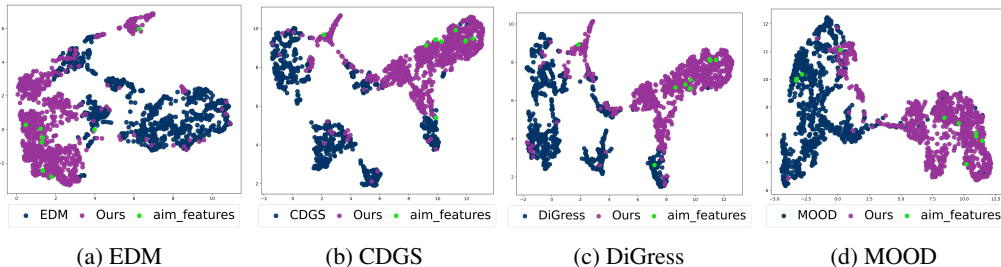


Figure 3: UMAP visualization of molecule generation results with our method compared to four mainstream methods using the target pair (NCI-H187, IC<sub>50</sub>=0.35).

### 4.3 Varying the regressor-free guidance strength experiment

Different conditional parameters can affect the sampling results during conditional molecule generation tasks. To investigate this, we conducted a regressor-free guidance strength experiment, applying our proposed regression-free guidance to conditionally generate molecules with an IC<sub>50</sub> of 0.4 for the cell line ES3 for resource consideration. In Fig. 4, we demonstrate our model’s sample quality effects under different guidance strengths  $w$ . In addition,  $w$  was selected non-uniformly from 0 to 10. The visualization comparison images for molecule generation with conditional  $w = 1.0$  and unconditional guidance  $w = 0.0$  can be found in Appendix Fig. 6.



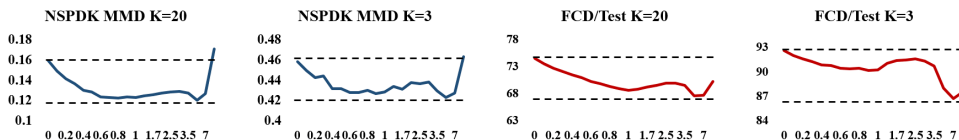


Figure 4: Visualization of regressor-free guidance strength trends. The x-axis represents the conditions’ intensity, where  $w = 0.0$  refers to non-guided models, while the y-axis represents the corresponding metric values.

As the conditional guidance strength increases, the molecule generation process gradually transitions toward the  $K$  target molecules feature values, but reaches the first extremal point at approximately  $w = 1$ . Subsequently, the generation performance deteriorates between  $1 < w < 3$ , and improves at approximately  $w = 5$ , reaching the second extremal point. Additionally, as  $K$  increases, the number of target molecules and the range of target  $IC_{50}$  scores expand, while the FCD and MMD metrics decrease. Thus, a smaller  $K$  represents a more stringent conditional generation task. In summary, we experimentally verified this paper’s main hypothesis: that regression-free guidance can steer generation models to generate directionally conditioned molecules, with two minimal guidance strength points  $w$  of 1 and 5.

#### 4.4 Ablation studies

Table 3: Our method’s ablation experiments involve the target pair (NCI-H187,  $IC_{50}=0.35$ ) with TopK values of 3, 5, 10, 15, and 20. The optimal results are indicated in **bold**, while the second-best results are underscored. The dash (-) signifies cases where both scenarios (not loading pre-trained models and unfreezing model weights) cannot occur simultaneously.

Mixed data training	Uncondition pre-trained	$B_1$ freezing	FCD	MMD	Validity w/o correction	Valid
✗	✗	✗	82.2 / 77.7 / 62.0 / 57.4 / 54.1	0.344 / 0.258 / 0.168 / 0.141 / 0.133	0.637	1
✗	✗	✓	-	-	-	-
✗	✓	✓	83.3 / 76.4 / 64.5 / 63.0 / 60.2	0.490 / 0.412 / 0.288 / 0.270 / 0.254	0.000	1
✗	✓	✗	<b>75.9 / 71.3 / 54.9 / 51.0 / 46.8</b>	<u>0.319</u> / <u>0.232</u> / <u>0.152</u> / <u>0.122</u> / <u>0.110</u>	0.494	1
✓	✗	✗	84.6 / 80.0 / 66.5 / 63.0 / 60.4	0.407 / 0.331 / 0.231 / 0.209 / 0.201	0.953	1
✓	✗	✓	-	-	-	-
✓	✓	✓	81.3 / 75.5 / 64.0 / 62.3 / 60.0	0.545 / 0.467 / 0.343 / 0.324 / 0.312	0.000	1
✓	✓	✗	<u>77.0</u> / <u>72.3</u> / <u>56.0</u> / <u>52.1</u> / <u>47.8</u>	<b>0.313</b> / <b>0.221</b> / <b>0.142</b> / <b>0.113</b> / <b>0.101</b>	0.586	1

We conducted ablation experiments to validate our method’s effectiveness in mixed data training, unconditional pre-training, and partial weight freezing.

**Mixed data training** refers to the practice of combining a small conditioned dataset and a large unconditioned one and jointly training them. Table 3 demonstrates that this effectively reduces the FCD and MMD between the generated and target molecules, and also improves the validity of molecules without post-correction.

**Unconditional pre-training** refers to training an unconditional generation model on datasets such as QM9 or ZINC250k, while simultaneously training a conditional model. While maintaining constant conditions, utilizing the unconditional model trained on the QM9 significantly improves the molecule generation quality. However, it affects the molecule validity during the initial generation process.

**Weight freezing** refers to the proposed DBControl model, which consists of two branches (i.e.,  $B_1$ ,  $B_2$ ). First,  $B_1$  undergoes unconditional training and is fine-tuned with  $B_2$  during mixed conditional training. During mixed conditional training, we set the  $B_1$  weights to remain unfrozen, distinguishing our method from other methods [51]. Various datasets play different roles, and simply freezing the weights of the pre-trained branch  $B_1$  may hinder effective data distribution learning. Furthermore, drug molecule features differ from those of images, and while molecular features may be similar,

their properties may not necessarily be. Therefore, weight freezing obstructs the channel for feature distribution transfer between large and small datasets designed for specific tasks.

## 5 Conclusion

This paper proposed a regressor-free guidance molecule generation model to ensure sampling within a more effective space, supporting the DRP task. Regressor-free guidance combines the score estimate of the DBControl model with the gradient of a regression controller one based on number labels. The regression controller model converts the target  $IC_{50}$  and cell line into text constrained by the CN-KG, effectively mapping the response value between drugs and cell lines. Additionally, to enhance noise prediction performance, we introduced the DBControl model for score estimation. The experimental results on real-world datasets during the DRP task demonstrated our method's effectiveness in de novo drug discovery, providing a novel and efficient solution for drug discovery.

## References

- [1] Brian DO Anderson. Reverse-time diffusion equation models. *Stochastic Processes and their Applications*, 12(3):313–326, 1982.
- [2] Peizhen Bai, Filip Miljković, Bino John, and Haiping Lu. Interpretable bilinear attention network with domain adaptation improves drug–target prediction. *Nature machine intelligence*, 5(2), 2023.
- [3] Amrita Basu, Nicole E Bodycombe, Jaime H Cheah, Edmund V Price, et al. An interactive resource to identify cancer genetic and lineage dependencies targeted by small molecules. *Cell*, 154(5):1151–1161, 2013.
- [4] Antoine Bordes, Nicolas Usunier, Alberto Garcia-Duran, Jason Weston, and Oksana Yakhnenko. Translating embeddings for modeling multi-relational data. *Advances in neural information processing systems*, 26, 2013.
- [5] Fabrizio Costa and Kurt De Grave. Fast neighborhood subgraph pairwise distance kernel. In *Proceedings of the 26th International Conference on Machine Learning*, pages 255–262. Omnipress; Madison, WI, USA, 2010.
- [6] Mathew J Garnett, Elena J Edelman, Sonja J Heidorn, et al. Systematic identification of genomic markers of drug sensitivity in cancer cells. *Nature*, 483(7391):570–575, 2012.
- [7] Rafael Gómez-Bombarelli, Jennifer N Wei, David Duvenaud, José Miguel Hernández-Lobato, Benjamín Sánchez-Lengeling, Dennis Sheberla, Jorge Aguilera-Iparraguirre, Timothy D Hirzel, Ryan P Adams, and Alán Aspuru-Guzik. Automatic chemical design using a data-driven continuous representation of molecules. *ACS central science*, 4(2):268–276, 2018.
- [8] Rafael Gómez-Bombarelli, Jennifer N Wei, David Duvenaud, José Miguel Hernández-Lobato, Benjamín Sánchez-Lengeling, Dennis Sheberla, Jorge Aguilera-Iparraguirre, Timothy D Hirzel, Ryan P Adams, and Alán Aspuru-Guzik. Automatic chemical design using a data-driven continuous representation of molecules. *ACS central science*, 4(2):268–276, 2018.
- [9] Nate Gruver, Samuel Stanton, Nathan Frey, Tim GJ Rudner, Isidro Hotzel, Julien Lafrance-Vanasse, Arvind Rajpal, Kyunghyun Cho, and Andrew G Wilson. Protein design with guided discrete diffusion. *Advances in Neural Information Processing Systems*, 36, 2024.
- [10] Jiaqi Guan, Wesley Wei Qian, Xingang Peng, Yufeng Su, Jian Peng, and Jianzhu Ma. 3d equivariant diffusion for target-aware molecule generation and affinity prediction. In *The Eleventh International Conference on Learning Representations*, 2022.
- [11] Jérôme Hert, John J Irwin, Christian Laggner, Michael J Keiser, and Brian K Shoichet. Quantifying biogenic bias in screening libraries. *Nature chemical biology*, 5(7):479–483, 2009.
- [12] Jonathan Ho and Tim Salimans. Classifier-free diffusion guidance. In *NeurIPS 2021 Workshop on Deep Generative Models and Downstream Applications*, 2021.
- [13] Emiel Hoogeboom, Victor Garcia Satorras, Clément Vignac, and Max Welling. Equivariant diffusion for molecule generation in 3d. In *International conference on machine learning*, pages 8867–8887. PMLR, 2022.
- [14] David Earl Hostallero, Lixuan Wei, Liewei Wang, Junmei Cairns, and Amin Emad. Preclinical-to-clinical anti-cancer drug response prediction and biomarker identification using tindl. *Genomics, Proteomics & Bioinformatics*, 21(3), 2023.
- [15] Han Huang, Leilei Sun, Bowen Du, and Weifeng Lv. Conditional diffusion based on discrete graph structures for molecular graph generation. In *Proceedings of the AAAI Conference on Artificial Intelligence*, volume 37, pages 4302–4311, 2023.
- [16] Lei Huang, Hengtong Zhang, Tingyang Xu, and Ka-Chun Wong. Mdm: Molecular diffusion model for 3d molecule generation. In *Proceedings of the AAAI Conference on Artificial Intelligence*, volume 37, pages 5105–5112, 2023.

- [17] John J Irwin, Teague Sterling, Michael M Mysinger, Erin S Bolstad, and Ryan G Coleman. Zinc: a free tool to discover chemistry for biology. *Journal of chemical information and modeling*, 52(7):1757–1768, 2012.
- [18] Likun Jiang, Changzhi Jiang, Xinyu Yu, Rao Fu, Shuting Jin, and Xiangrong Liu. Deeptta: a transformer-based model for predicting cancer drug response. *Briefings in bioinformatics*, 23(3):bbac100, 2022.
- [19] José Jiménez-Luna, Miha Skalic, and Nils Weskamp. Benchmarking molecular feature attribution methods with activity cliffs. *Journal of Chemical Information and Modeling*, 62(2):274–283, 2022.
- [20] Wengong Jin, Regina Barzilay, and Tommi Jaakkola. Junction tree variational autoencoder for molecular graph generation. In *International conference on machine learning*, pages 2323–2332. PMLR, 2018.
- [21] Jaehyeong Jo, Seul Lee, and Sung Ju Hwang. Score-based generative modeling of graphs via the system of stochastic differential equations. In *Proceedings of the 39th International Conference on Machine Learning*, volume 162 of *Proceedings of Machine Learning Research*, pages 10362–10383. PMLR, 17–23 Jul 2022.
- [22] Jaehyeong Jo, Dongki Kim, and Sung Ju Hwang. Graph generation with destination-driven diffusion mixture. In *ICLR 2023-Machine Learning for Drug Discovery workshop*, 2023.
- [23] Christiaan Klijn, Steffen Durinck, Eric W Stawiski, et al. A comprehensive transcriptional portrait of human cancer cell lines. *Nature biotechnology*, 33(3):306–312, 2015.
- [24] Dai Kusumoto, Tomohisa Seki, Hiromune Sawada, Akira Kunitomi, Toshiomi Katsuki, Mai Kimura, Shogo Ito, Jin Komuro, Hisayuki Hashimoto, Keiichi Fukuda, et al. Anti-senescent drug screening by deep learning-based morphology senescence scoring. *Nature communications*, 12(1):257, 2021.
- [25] Seul Lee, Jaehyeong Jo, and Sung Ju Hwang. Exploring chemical space with score-based out-of-distribution generation. In *International Conference on Machine Learning*, pages 18872–18892. PMLR, 2023.
- [26] Hyunsoo Lee, Minsoo Kang, and Bohyung Han. Conditional score guidance for text-driven image-to-image translation. *Advances in Neural Information Processing Systems*, 36, 2024.
- [27] Kun Li and Wenbin Hu. Cldr: Contrastive learning drug response models from natural language supervision. *ArXiv*, abs/2312.10707, 2023.
- [28] Guodong Li, Chun Wu, Dik-Lung Ma, and Chung-Hang Leung. Drug screening strategies using metal-based luminescent probes. *TrAC Trends in Analytical Chemistry*, 139:116270, 2021.
- [29] Haoying Li, Yifan Yang, Meng Chang, Shiqi Chen, Huajun Feng, Zhihai Xu, Qi Li, and Yueting Chen. Srdiff: Single image super-resolution with diffusion probabilistic models. *Neurocomputing*, 479:47–59, 2022.
- [30] Xiaoqian Lin, Xiu Li, and Xubo Lin. A review on applications of computational methods in drug screening and design. *Molecules*, 25(6):1375, 2020.
- [31] Phillip Lippe and Efstratios Gavves. Categorical normalizing flows via continuous transformations. In *International Conference on Learning Representations*, 2020.
- [32] Qi Liu, Miltiadis Allamanis, Marc Brockschmidt, and Alexander Gaunt. Constrained graph variational autoencoders for molecule design. *Advances in neural information processing systems*, 31, 2018.
- [33] Hong Liu-Seifert, Scott Andersen, Michael Case, JonDavid Sparks, Karen C Holdridge, Alette M Wessels, Suzanne Hendrix, Paul Aisen, and Eric Siemers. Statistical properties of continuous composite scales and implications for drug development. *Journal of biopharmaceutical statistics*, 27(6):1104–1114, 2017.

- [34] Youzhi Luo, Keqiang Yan, and Shuiwang Ji. Graphdf: A discrete flow model for molecular graph generation. In *International conference on machine learning*, pages 7192–7203. PMLR, 2021.
- [35] Asher Mullard. The drug-maker’s guide to the galaxy. *Nature*, 549(7673):445–447, 2017.
- [36] Xingang Peng, Jiaqi Guan, Qiang Liu, and Jianzhu Ma. Moldiff: addressing the atom-bond inconsistency problem in 3d molecule diffusion generation. In *Proceedings of the 40th International Conference on Machine Learning*, pages 27611–27629, 2023.
- [37] Pavel G Polishchuk, Timur I Madzhidov, and Alexandre Varnek. Estimation of the size of drug-like chemical space based on gdb-17 data. *Journal of computer-aided molecular design*, 27:675–679, 2013.
- [38] Kristina Preuer, Philipp Renz, Thomas Unterthiner, Sepp Hochreiter, and Gunter Klambauer. Fréchet chemnet distance: a metric for generative models for molecules in drug discovery. *Journal of chemical information and modeling*, 58(9):1736–1741, 2018.
- [39] Raghunathan Ramakrishnan, Pavlo O Dral, Matthias Rupp, and O Anatole Von Lilienfeld. Quantum chemistry structures and properties of 134 kilo molecules. *Scientific data*, 1(1):1–7, 2014.
- [40] Matthew G Rees, Brinton Seashore-Ludlow, Jaime H Cheah, et al. Correlating chemical sensitivity and basal gene expression reveals mechanism of action. *Nature chemical biology*, 12(2):109–116, 2016.
- [41] Lars Ruddigkeit, Ruud Van Deursen, Lorenz C Blum, and Jean-Louis Reymond. Enumeration of 166 billion organic small molecules in the chemical universe database gdb-17. *Journal of chemical information and modeling*, 52(11):2864–2875, 2012.
- [42] Yang Song, Jascha Sohl-Dickstein, Diederik P Kingma, Abhishek Kumar, Stefano Ermon, and Ben Poole. Score-based generative modeling through stochastic differential equations. In *International Conference on Learning Representations*, 2020.
- [43] Hongda Sun, Shufang Xie, Shuqi Li, Yuhan Chen, Ji-Rong Wen, and Rui Yan. Debiased, longitudinal and coordinated drug recommendation through multi-visit clinic records. *Advances in Neural Information Processing Systems*, 35:27837–27849, 2022.
- [44] Daniele Turi and Jan Rutten. On the foundations of final coalgebra semantics: non-well-founded sets, partial orders, metric spaces. 8:481–540, 1998.
- [45] Clément Vignac, Igor Krawczuk, Antoine Siraudin, Bohan Wang, Volkan Cevher, and Pascal Frossard. Digress: Discrete denoising diffusion for graph generation. In *Proceedings of the 11th International Conference on Learning Representations*, 2023.
- [46] Lemeng Wu, Chengyue Gong, Xingchao Liu, Mao Ye, and Qiang Liu. Diffusion-based molecule generation with informative prior bridges. *Advances in Neural Information Processing Systems*, 35:36533–36545, 2022.
- [47] Minkai Xu, Alexander S Powers, Ron O Dror, Stefano Ermon, and Jure Leskovec. Geometric latent diffusion models for 3d molecule generation. In *Proceedings of the 40th International Conference on Machine Learning*, pages 38592–38610, 2023.
- [48] Minkai Xu, Alexander S Powers, Ron O Dror, Stefano Ermon, and Jure Leskovec. Geometric latent diffusion models for 3d molecule generation. In *International Conference on Machine Learning*, pages 38592–38610. PMLR, 2023.
- [49] Wanjuan Yang, Jorge Soares, Patricia Greninger, Elena J Edelman, Howard Lightfoot, Simon Forbes, Nidhi Bindal, Dave Beare, James A Smith, I Richard Thompson, Sridhar Ramaswamy, P Andrew Futreal, Daniel A Haber, Michael R Stratton, Cyril Benes, Ultan McDermott, and Mathew J Garnett. Genomics of drug sensitivity in cancer (gdsc): a resource for therapeutic biomarker discovery in cancer cells. *Nucleic acids research*, 41(Database issue):D955–61, January 2013.

- [50] Soojung Yang, Doyeong Hwang, Seul Lee, Seongok Ryu, and Sung Ju Hwang. Hit and lead discovery with explorative rl and fragment-based molecule generation. *Advances in Neural Information Processing Systems*, 34:7924–7936, 2021.
- [51] Lvmin Zhang, Anyi Rao, and Maneesh Agrawala. Adding conditional control to text-to-image diffusion models. In *Proceedings of the IEEE/CVF International Conference on Computer Vision*, pages 3836–3847, 2023.

**Organization** The appendix is structured as follows: In Section A, the authors present the proposed framework for regressor-free guidance molecule generation, delineating its three training stages. Section B delves into related work, emphasizing the significance and practical implications of regressor-guidance molecule generation. Section D offers proofs for the three propositions formulated in this paper. Experimental details about the generation tasks are expounded upon in Section D, alongside supplementary experimental results. Finally, Section E provides visual representations of the generated molecules and graphs.

## A Model details

### A.1 Framework of regressor-free guidance molecule generation

We propose the regressor-free guidance molecule generation, which involves three training stages.

The first stage is the training of the unconditional molecule generation model. Large-scale unconditional datasets such as QM9 [39], GDB-17 [41], and ZINC250k [17] are used for training. During this phase, the model, specifically the noise prediction model, is trained without incorporating any specific condition information, focusing solely on learning the fundamental patterns and structures of molecule generation.

The second stage is the training of the regression controller model. Specific task datasets, such as GDSCv2 for the drug–cell line response task, are used. In this phase, contrastive learning methods are employed to train the regression controller model, converting the regression labels of drug information into text. A drug encoder and a text encoder work together to optimize this conversion process, ensuring that the response label between the drugs and the cell lines are effectively represented.

The third stage is the training and sampling with the conditional noise prediction model. This phase uses a mixture of conditional and unconditional datasets to train the noise prediction model, ensuring it can generate valid molecules under specific conditions. During the sampling process, the text conditions generated by the regression controller model guide the molecule generation process. This method employs a regressor-free guidance generation, similar to classifier-free diffusion guidance [12].

This framework integrates the training of the unconditional molecule generation model, the training of the regression controller model, and the training and sampling of the conditional noise prediction model. This method can sample within a smaller range near specific response values, thereby improving generation efficiency while also increasing the success rate of drug discovery.

### A.2 Schematic of DBControl model

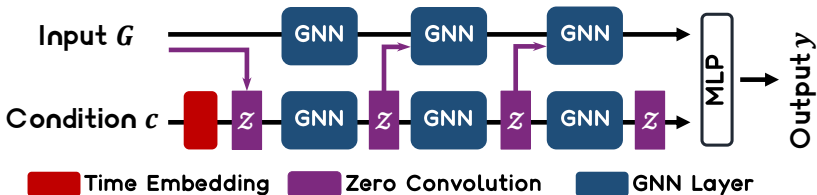


Figure 5: Schematic of the DBControl.

The DBControl model, as shown in Figure 5, consists of three main components: the input layer  $G$  representing the molecular graph, the condition vector  $c$  specifying the desired properties or constraints, and the output layer  $y$  generating the molecule. The model operates in three stages:

1. **Graph encoder:** The input graph  $G$  is encoded into a fixed-dimensional representation using a graph encoder.
2. **Condition processing:** The condition vector  $c$  is processed through a neural network to extract relevant features and ensure compatibility with the graph representation.
3. **Zero convolution:** Through zero convolution, the input graph  $G$  is first encoded, and the condition  $c$  is fused with  $G$ .

This schematic illustrates the architecture and flow of information within the DBControl model. In our method, we create two DBControl models to predict noise for both  $\mathbf{X}$  and  $\mathbf{A}$ . It is worth noting that when the noise prediction for  $\mathbf{X}$ , the embedding of time  $t$  is mixed with condition  $\mathbf{c}$  to make the model sensitive to different time embeddings of condition  $\mathbf{c}$  during different time steps  $t$ .

## B Related work

Recently, score-based generative models have been applied to image inpainting [42], super-resolution [29], and image translation [26]. However, applying these methods to the conditional generation of molecules poses several challenges. Firstly, due to the complex dependencies between nodes and edges [36], it is necessary to simultaneously consider the validity of both types of information and the relationships between them [21]. Additionally, when generating molecules under specific conditions, it is essential to consider the molecular property information [46]. The prevalence of activity cliffs [19] indicates that generating molecules similar to the target molecule does not guarantee similar properties.

On this basis, generalized property-based molecule generation methods can be categorized into two types. One type solely describes molecular properties (such as chemical, physical, and biological properties) [48, 16], while the other type describes interactions, connections, or associations between molecules (including interaction forces [43], reactions with cell lines [14], and protein-ligand binding patterns [2]). Existing diffusion-based molecule generation methods essentially guide generation through classification [45], yet these properties naturally exist in continuous numerical (regression) form.

The generation models based on classification guidance and regression guidance exhibit fundamental differences in molecule generation. Models guided by classification primarily employ the classifier to direct molecule generation, categorizing molecules into different classes or sets. This method is typically suitable for generating samples for classification tasks [10], such as distinguishing between drug and non-drug molecules. In contrast, regressor-based guidance method aim to generate molecules with specific numerical properties or response values. This method focuses more on the numerical features of molecules, such as predicting drug activity or optimizing specific molecular properties. Therefore, the choice between these guidance types depends on the specific application requirements and generation goals. In the majority of drug screening tasks [28, 30], priority is given to molecules with superior properties determined through the numerical ranking of molecular attributes. This prioritization favors molecules exhibiting better properties, as assessed through virtual calculations [24]. Consequently, regressor-free guidance generation models are crucial in a series of tasks for drug screening.

## C Proof of propositions

**Proposition 1 (Main proposition)** For any  $C_{\text{aim}} \in (0, 1)$ , then  $\|S_{cls}\| \geq \|S_{reg}\|$  exists.

*Proof.*  $\xi$  is the number of valid digits, and  $\xi \in \mathbb{N}$ . The significant figures are preserved by rounding off, hence the sampling radius of reg at  $C_{\text{aim}}$  point is  $\frac{10^{-\xi}}{2}$ . Then, we have:

$$\begin{aligned} \|S_{cls}\| &= (T \pm \varepsilon_1) - (0 \pm \varepsilon_1) \\ &= T \\ \|S_{reg}\| &= (C_{\text{aim}} + \frac{10^{-\xi}}{2} \pm \varepsilon_2) - (C_{\text{aim}} - \frac{10^{-\xi}}{2} \pm \varepsilon_2) \\ &= 10^{-\xi} \\ \|S_{cls}\| - \|S_{reg}\| &= T - 10^{-\xi} \\ &\geq 0. \end{aligned}$$

**Proposition 2 (Uniqueness of  $C_{\text{aim}}$  Representation)** For any  $\lambda \in [0, 1]$ , and  $\lambda \neq C_{\text{aim}}$ , then we say that  $\Theta(C_{\text{aim}}) \neq \Theta(\lambda)$ .



*Proof.* We will prove Lemma 2 by contradiction. Suppose there exists a  $\lambda \in [0, 1]$ ,  $\lambda \neq C_{\text{aim}}$ , and then  $\Theta(C_{\text{aim}}) = \Theta(\lambda)$ . Then, we utilize Proposition 3 to derive a variant of the left-hand side:

$$\begin{aligned}\Theta(C_{\text{aim}}) &= \Theta(C_{\text{aim}} + 1) + \mathbf{1} + \varepsilon_3 \\ &= \Theta(C_{\text{aim}} + 2) + 2\mathbf{1} + 2\varepsilon_3 \\ &\vdots \\ &= \Theta(\lambda) + |\lambda - C_{\text{aim}}|\mathbf{1} + |\lambda - C_{\text{aim}}|\varepsilon_3,\end{aligned}$$

Then, we have:

$$\Theta(\lambda) = \Theta(\lambda) + |\lambda - C_{\text{aim}}|\mathbf{1} + |\lambda - C_{\text{aim}}|\varepsilon_3. \quad (13)$$

The equation 13 holds under two conditions. First,  $\lambda = C_{\text{aim}}$ , which contradicts the assumption of this proposition. Second,  $\mathbf{1} + \varepsilon_3 = \mathbf{0}$ . Since  $\varepsilon_3$  is much smaller than  $\mathbf{1}$ , and  $|\mathbf{1}| = 1$ , this solution is not valid. Considering both solutions contradict the known conditions, the negative proposition of Proposition 2 is false, thus Proposition 2 holds.

**Proposition 3 (Equal interval representation of  $\Theta$ )** For any  $\xi$ , a perturbation  $\varepsilon_3$  exist to make  $\Theta(V[i]) - \Theta(V[i + 1]) = \mathbf{1} + \varepsilon_3$ .

*Proof.* To consider  $\mathcal{L}_{\text{KGE}}$  with the squared euclidean distance as dissimilarity function [4], we have:

$$\mathcal{L}_{\text{KGE}} = \sum_{(h,l,t) \in S} [\gamma + d(\mathbf{h} + \mathbf{l}, \mathbf{t}) - d(\mathbf{t} + \mathbf{l}, \mathbf{h})]_+. \quad (14)$$

Then,  $\Theta(V[i + 1])$  and  $\Theta(V[i])$  can be represent as  $\mathbf{h}$  and  $\mathbf{t}$ . As the translation-based model proposed by [4],  $\mathbf{t}$  should be a nearest neighbor of  $\mathbf{h} + \mathbf{l}$ , i.e.  $\mathbf{h} + \mathbf{l} \approx \mathbf{t}$ . Then, the  $\Theta(V[i]) + \mathbf{1} \approx \Theta(V[i + 1])$ . By utilizing  $\varepsilon_3$  to denote the error term of  $\mathcal{L}_{\text{KGE}}$ , we have  $\Theta(V[i + 1]) + \mathbf{1} + \varepsilon_3 = \Theta(V[i])$ .

## D Experimental details

### D.1 Baselines

We selected representative diffusion methods with high performance for molecule generation in recent years, including GDSS [21], EDM [13], CDGS [15], GeoLDM [47], DiGress [45], MOOD [25], GruM-2D [22].

### D.2 Datasets

The dataset information, summarized in Table 4 and Table 5, comprises openly accessible datasets available online for academic purposes. All datasets listed are freely downloadable and intended for academic use.

Table 4: Unconditional Molecule dataset information.

Dataset	Number of molecules	Number of nodes	Number of node types	Number of edge types
ZINC250k [17]	249,455	$6 \leq  V  \leq 38$	9	3
QM9 [39]	133,885	$1 \leq  V  \leq 9$	4	3
GDB-17 [41]	166,443,860,262	-	17	-

### D.3 Settings

We use NVIDIA RTX A6000 for model training, requiring support for 48GB of VRAM and a memory capacity of no less than 128 GB. The maximum number of atoms accepted as input molecules and also

Table 5: Datasets for DRP tasks, where sensitivity assay means the method for calculating the  $IC_{50}$ .

Dataset	GDSCv1	GDSCv2	CTRPv1	CTRPv2	GCSI
	[6]	[49]	[3]	[40]	[23]
Total Number	258196	152839	30545	130855	6178
Drug Type Number	309	223	354	545	43
Average per drug	835	655	86	240	143
Cell Type Number	968	990	184	589	366
Sensitivity assay	Syto60	CellTitreGlo	CellTitreGlo	CellTitreGlo	CellTitreGlo
Model Evaluation	Hold-out	Hold-out	K-Flod	Hold-out	K-Flod

the maximum number of atoms in generated molecules is denoted as MNN, MFN is the maximum number of atom types.

**The regression controller model.** The margin for  $\mathcal{L}_{KGE}$  is set to 1.0, the entity dimension (dim) is set to 128, and the learning rate is set to 0.0001. For  $\mathcal{L}_{KGE}$ , the batch size is 1024, the MNN is 100, and the MFN is 10. The Adam optimizer is used with a weight decay of 0.05.

**The dual-branch controlled noise prediction model.** In the diffusion phase, the DBControl model undergoes mixed training with a learning rate of 0.0001 and a weight decay of 0.0005 using the Adam optimizer. The batch size is set to 512, the MNN set to 100, and MFN to 10. The model is initialized with pre-trained weights from QM9, with the pre-training parameters being identical to those used in the conditional mixed training. In the sampling phase, the signal-to-noise ratio (SNR) is set to 0.2, and the scale epsilon is 0.7. The total number of time steps is 1000.

**Compute resource requirements and time consumption.** During diffusion, with a batch size of 512, approximately 30,000 MB of memory is required, and it takes 96 hours for 500 epochs. Sampling 1000 molecules requires about 10,000 MB of memory and 0.5 hours.

#### D.4 Metrics

We evaluate the quality of the 1,000 generated molecules with the following metrics. FCD [38] evaluates the distance between the training and generated sets using the activations of the penultimate layer of the ChemNet. (NSPDK) MMD [5] is the MMD between the generated molecules and test molecules which takes into account both the node and edge features for evaluation. Specifically, FCD measures the ability in the view of molecules in chemical space, while NSPDK MMD measures the ability in the view of the graph structure [21].

#### D.5 Error assessment

We conducted 5 random seed sampling experiments for each of the 4 cell lines involved in the overall experiment in Section 4.2 to assess the errors of our method (as shown in Tables 6, 7, 8, and 9). These tables displays the mean and variance of the sampling results for the FCD and MMD metrics over 5 random seeds. Both the mean and variance decrease as TopK increases. A smaller TopK indicates more stringent evaluation criteria; for instance, TopK=1 implies that the molecular generation method must be similar to a single target molecule and must be constrained under the conditions of the target cell line and target  $IC_{50}$ . The consistent trend in mean and variance also reflects the alignment of our method with established facts and its effectiveness.

Our coefficient of variation, approximately 0.041%, 0.028%, 0.037%, 0.036%, 0.034% for FCD and 0.002%, 0.003%, 0.002%, 0.001%, 0.002% for MMD, respectively, indicates that our method produces molecules with high stability and low error.

## E Visualization

We visualize the features of molecule sampling under different conditions to compare the sampling effects. Taking the NCI-H187 cell line (ID: 688007) as an example, the target  $IC_{50}$  is set to 0.35.

Table 6: Five random seed experiments regarding the target  $IC_{50}$  score at 0.4 for the cell line ES5 at  $T = 1000$  time steps.

Metrics	TopK	Seed					Mean	Var ( $\pm$ )
		40	41	42	43	44		
FCD	3	68.815	69.241	68.867	68.997	68.977	68.9794	0.027103
	5	63.321	63.547	63.371	63.358	63.433	63.406	0.007841
	10	53.549	53.84	53.653	53.731	53.966	53.7478	0.026226
	15	50.716	50.987	50.711	50.823	50.998	50.847	0.019659
	20	55.003	55.242	54.977	55.057	55.271	55.11	0.018823
MMD	3	0.33	0.324	0.327	0.329	0.326	0.3272	5.7E-06
	5	0.228	0.226	0.226	0.228	0.226	0.2268	1.2E-06
	10	0.136	0.137	0.135	0.136	0.136	0.136	5E-07
	15	0.117	0.117	0.116	0.116	0.117	0.1166	3E-07
	20	0.107	0.108	0.107	0.106	0.107	0.107	5E-07

Table 7: Five random seed experiments regarding the target  $IC_{50}$  score at 0.4 for the cell line Hs-578-T at  $T = 1000$  time steps.

Metrics	TopK	Seed					Mean	Var ( $\pm$ )
		40	41	42	43	44		
FCD	3	98.5	98.16	98.384	98.241	98.039	98.2648	0.033016
	5	68.985	68.784	68.811	69.016	68.634	68.8460	0.024559
	10	67.985	67.936	67.714	68.061	67.628	67.8648	0.034207
	15	64.599	64.513	64.35	64.653	64.226	64.4682	0.031475
	20	60.327	60.328	60.101	60.334	60.008	60.2196	0.023803
MMD	3	0.294	0.295	0.299	0.296	0.299	0.2966	5.3E-06
	5	0.199	0.198	0.2	0.2	0.201	0.1996	1.3E-06
	10	0.159	0.157	0.158	0.161	0.159	0.1588	2.2E-06
	15	0.13	0.128	0.129	0.13	0.129	0.1292	7E-07
	20	0.109	0.108	0.109	0.11	0.11	0.1092	7E-07

Table 8: Five random seed experiments regarding the target  $IC_{50}$  score at 0.4 for the cell line ES3 at  $T = 100$  time steps.

Metrics	TopK	Seed					Mean	Var ( $\pm$ )
		40	41	42	43	44		
FCD	3	76.997	76.962	76.928	76.512	76.723	76.8244	0.041833
	5	71.863	71.965	71.879	71.593	71.637	71.7874	0.026515
	10	55.041	55.094	55.000	54.934	54.867	54.9872	0.007936
	15	51.622	51.546	51.649	51.405	51.410	51.5264	0.01321
	20	47.072	47.133	47.113	46.923	46.949	47.0380	0.009238
MMD	3	0.306	0.304	0.303	0.306	0.308	0.3054	3.8E-06
	5	0.208	0.210	0.210	0.214	0.212	0.2108	5.2E-06
	10	0.130	0.129	0.129	0.129	0.131	0.1296	8E-07
	15	0.104	0.103	0.103	0.103	0.106	0.1038	1.7E-06
	20	0.092	0.091	0.091	0.091	0.094	0.0918	1.7E-06

Table 9: Five random seed experiments regarding the target  $IC_{50}$  score at 0.35 for the cell line NCI-H187 at  $T = 1000$  time steps.

Metrics	TopK	Seed					Mean	Var ( $\pm$ )
		40	41	42	43	44		
FCD	3	90.54	90.541	90.225	90.352	90.7	90.4716	0.034194
	5	86.372	86.412	86.269	86.22	86.621	86.3788	0.024271
	10	76.51	76.386	76.189	76.257	76.555	76.3794	0.024792
	15	74.333	74.307	74.132	74.043	74.401	74.2432	0.02237
	20	68.846	68.802	68.564	68.526	68.895	68.7266	0.028745
MMD	3	0.432	0.431	0.428	0.429	0.426	0.4292	5.7E-06
	5	0.282	0.275	0.273	0.274	0.271	0.2750	1.75E-05
	10	0.186	0.179	0.178	0.178	0.178	0.1798	1.22E-05
	15	0.151	0.148	0.146	0.148	0.146	0.1478	4.2E-06
	20	0.128	0.123	0.123	0.124	0.123	0.1242	4.7E-06

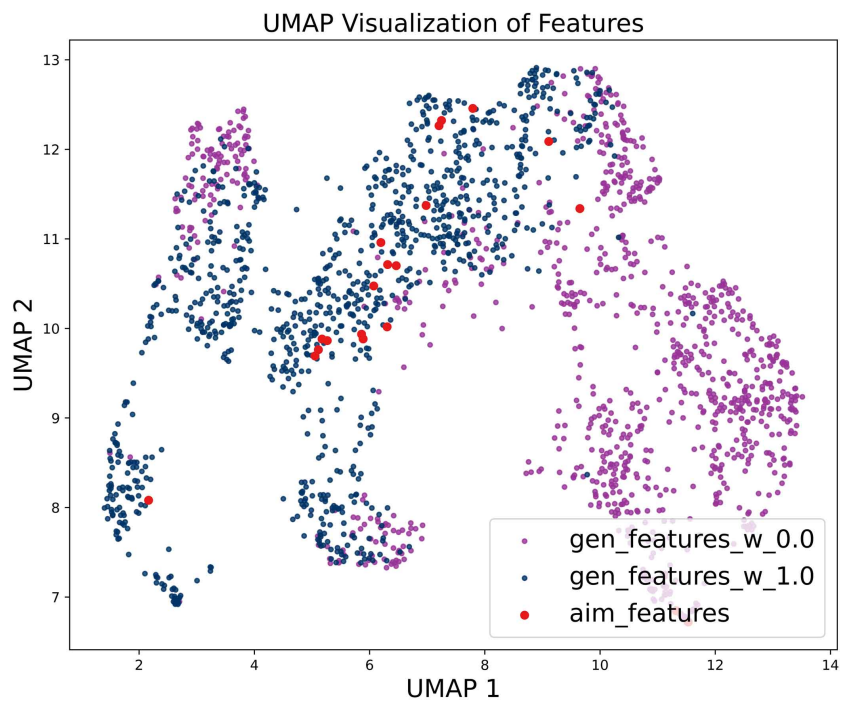
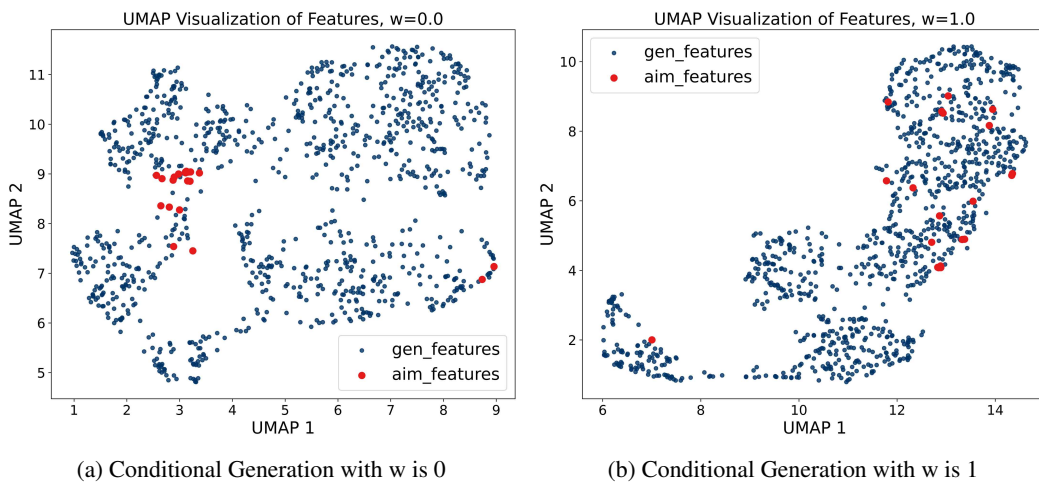


Figure 6: Molecule generation: conditional vs. unconditional guidance

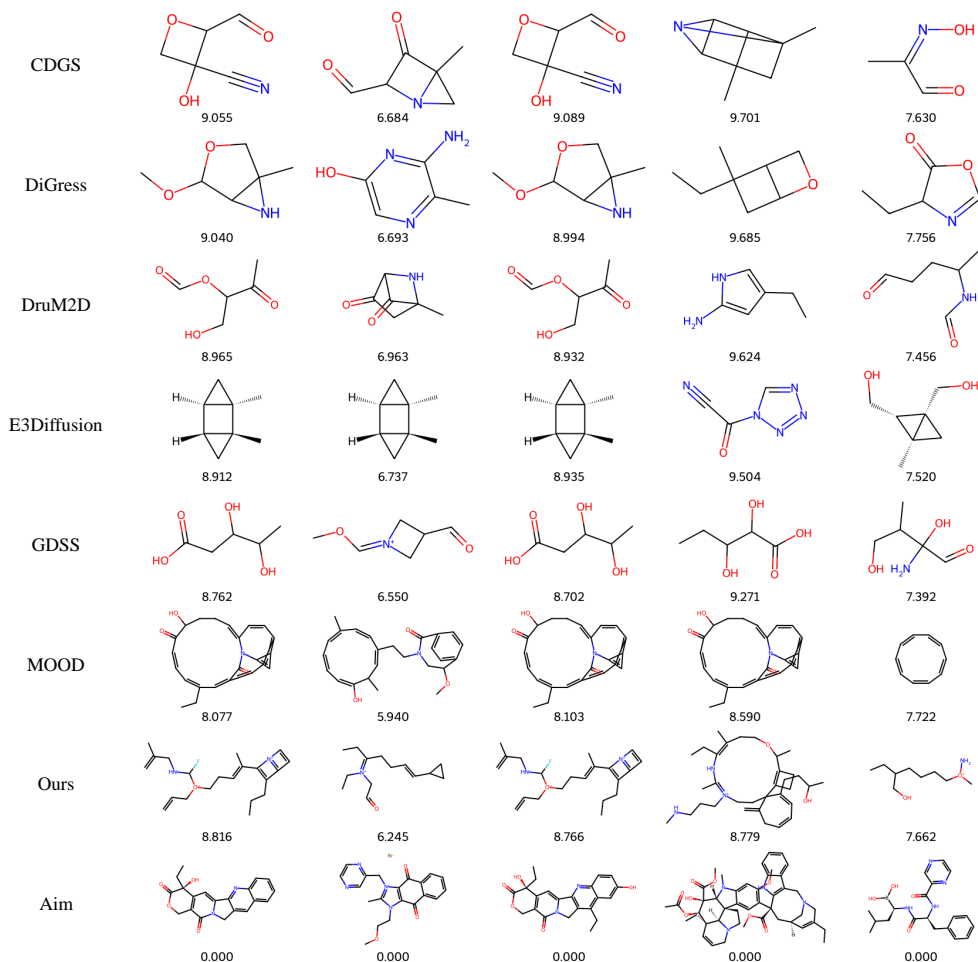


Figure 7: The comparison of molecule images for seven diffusion-based molecule generation methods. Among 1,000 generated molecules using the target pair (NCI-H187,  $IC_{50}=0.35$ ), the one most similar to the target molecule is selected.

The reason for setting it to 0.35 instead of the common 0.4 in previous cases is that this cell line has experimental data around 0.35. Fig. 6(a) and Fig. 6(b) show the feature distributions of generated molecules and target molecules under condition strengths  $w = 0$  and  $w = 1$ , respectively. We selected the 20 target molecules nearest to the  $IC_{50}$  in the molecular reaction data corresponding to this cell line in the dataset. Features were extracted using FCDNet [38] with a dimensionality of 512, followed by dimensionality reduction by Uniform Manifold Approximation and Projection (UMAP). When the condition strength  $w = 1$ , the feature distribution of generated molecules is more clustered around the target molecules compared to  $w = 0$ .

In addition, Fig. 6(c) uses a similar method to generate feature distribution plots. We simultaneously reduce the dimensionality of  $w = 0$  and  $w = 1$  cases to the same feature space for visualization. The condition-guided generation results are closer to the target molecules compared to the unconditional generation results. Even in the lower left corner of Fig. 6(c), where the target molecules are located, the condition-guided generated molecules are also distributed.

Fig. 7 illustrates the structures of the five molecules most similar to the five target molecules generated by seven different methods. We observe that although MOOD [25] shows advantages in similarity, the generated molecules all exhibit large cyclic structures of carbon, which significantly deviate from the structure of the target molecules, making it uncertain whether they are effective molecules. Other

methods generate molecules with distinct substructures; for instance, E3Diffusion [13] generates molecules with similar scaffolds, while GDSS [21] generates molecules consisting mainly of single carbon chains. Evaluating molecular generation performance solely based on metrics is not reliable, and visualizing the generated results cannot serve as an objective measure. However, based on the overall structure of the molecules, our method demonstrates strong competitiveness, whether assessed by metrics or visualized results.

## F Future work and limitations

### F.1 Limitations

While our work introduces a novel method and demonstrates significant improvements in the field of conditional molecular graph generation for DRP tasks, there are several limitations to acknowledge:

**Lack of Wet Lab Validation.** Our method has not yet been validated through wet lab experiments. This limits the practical verification of the generated molecules’ efficacy and safety in real-world biological settings. However, conducting wet lab experiments poses significant challenges for us due to the unique nature of the molecular generation field. Wet lab experiments require teams to have access to facilities for molecular synthesis, cell culture, and biological experimentation. These experiments are costly and have extremely long trial periods. Even the largest drug discovery company globally finds it difficult to afford and turns to computer-aided drug discovery instead.

**Evaluation Metrics.** While we demonstrate improved performance using standard evaluation metrics (FCD and MMD, see Appendix D.4), these metrics may not capture all aspects of model performance, particularly in real-world applications. Additional metrics and qualitative assessments could provide a more comprehensive evaluation of the model’s utility and effectiveness.

**Computational Resources.** The proposed method, including regressor-free guidance and the DBControl model, involves complex computations that demand significant computational resources, potentially limiting its feasibility in resource-constrained environments.

### F.2 Future work

Our proposed regressor-free guidance molecule generation will significantly contribute to accelerating the pace of drug discovery to a considerable extent. This is because we fully consider the challenges of drug discovery in molecular preliminary screening. Existing methods, which are limited to unconditional generation or classification-guided generation, fall short of practical application. Real-world applications require models with numerical, ranking, and recommendation capabilities. Therefore, we call for more scholars to explore regression tasks. In our future work, we will incorporate additional conditions into this method and validate the effectiveness of the method through wet experiments.